Tunable wrinkle modes of core-shell polymer fibers in electrospinning

Journal of Physics Communications

PAPER

Tunable wrinkle modes of core-shell polymer fibers in electrospinning

Mojtaba Ahmadi and Xiang-Fa Wu

Department of Mechanical Engineering, North Dakota State University, Fargo, North Dakota, 58108, United States of America

E-mail: Xiangfa.Wu@ndsu.edu

Keywords: surface wrinkle, nonlinear elasticity, buckling, numerical simulation, polymer fibers, electrospinning, nanomanufacturing

OPEN ACCESS

RECEIVED
1 February 2019

REVISED
11 March 2019

ACCEPTED FOR PUBLICATION
25 March 2019

PUBLISHED
8 April 2019

Abstract

Wrinkled surfaces are commonly observed on ultrathin polymer fibers produced in electrospinning process. This paper is to formulate a continuum mechanics model to explore dependencies of surface wrinkling of electrospun core–shell polymer fibers enwrapped with hard cores upon the thickness and stiffness of the glassy shell and inner soft sol-gel layer. The study provides a rational basis of surface wrinkling in electrospun polymer fibers and the technical strategies to regulate the electrospinning process for producing ultrathin polymer fibers with tunable surface morphologies for broad applications (e.g., oil-water separation, tissue scaffolding, etc).

1. Introduction

Electrospinning provides a viable technique for low-cost fabrication of ultrathin continuous fibers of polymers and polymer-derived carbon, silicon, metals, metal oxides, ceramics, etc with the diameters ranging from a few nanometers to micrometers [1–5]. As a type of unique one-dimensional (1D) micro/nanofibrous material with well tailorable diameters, microstructures and surface morphologies, electrospun fibers have found promising applications in nanocomposites, high-grade gas and liquid filtration, wound dressing, drug delivery, tissue engineering, and energy harvesting, conversion and storage, among others [6–14]. The unique continuity, large specific surface area (~1–100 $m^2\ g^{-1}$), and tunable surface morphologies are the superior structural advantages of electrospun fibers. In a typical electrospinning process, under the action of electrostatic force, the polymer solution jet undergoes a vital whipping process [15–18], in which the jet is elongated extremely and solvent evaporates vigorously. The fast drying due to rapid solvent evaporation out of the thin electrospun jet may result in two competing fiber surface morphologies, i.e., the porous fiber surface due to thermodynamic phase separation of the binary solvent-polymer system [19, 20] as well as the circumferentially wrinkled fiber surface due to mechanical destabilization of the glassy surface layer after radially uneven drying induced strain mismatch (see figure 1) [21, 22]. The latter are different from their counterparts of longitudinal surface winkles that were observed in electrospun thermoplastic nanofibers under uniaxial tension [23, 24] and quantitatively interpolated by continuum mechanics models and molecular dynamics simulations [25–27].

Model-based simulation of solvent evaporation from a polymer jet in electrospinning has confirmed the drastically uneven radial distribution of solvent in the jet with the diameter in the range of a few micrometers [28]. Thus, the surface layer of an electrospun jet starts drying (solidification) instantaneously after the jet leaves the nozzle while the core of the jet is nearly intact up to seconds in the case of a typical electrospinning process. The theoretical prediction provides a rational basis of ribbon-like structures observed in electrospun fibers by Koombhongse *et al* [21]. They further proposed a kinematic mechanism responsible for the formation of shaped fibers in electrospinning such that the atmospheric pressure serves as the driving force to collapse the fast-drying glassy skin (shell) initially solidified on the jet surface. Such a mechanism is applicable to interpolate the wrinkled surface morphologies in electrospun fibers [22]. Therefore, in principle, the surface wrinkling of electrospun fibers can be tuned via adjusting the process and material parameters of electrospinning such as the initial jet diameter (i.e., the nozzle outlet diameter), the solvent concentration, etc. For instance, the surface wettability (against water) of electrospun polystyrene (PS) nanofiber membranes can be tuned via controlling the diameter

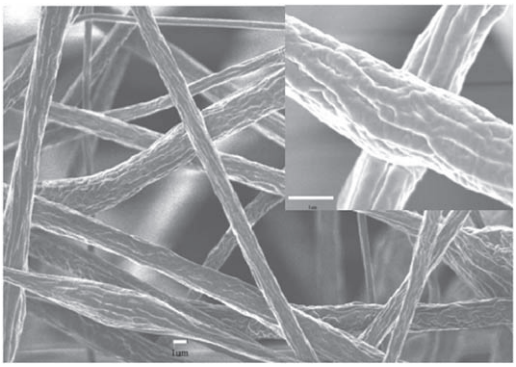

Figure 1. SEM micrograph of circumferential wrinkles on electrospun polystyrene (PS) fibers prepared from 10 wt% PS/tetrahydrofuran (THF) solution.

and drying-induced surface wrinkle modes of the ultrathin PS fibers, which was made possible through adjusting the solvent [e.g., tetrahydrofuran (THF)] fraction of the PS/THF solution used in electrospinning. The PS nanofiber membranes have demonstrated promising applications for effective water filtration and oil-water separation [29–31].

In addition, within the framework of continuum mechanics, initiation of surface wrinkling in electrospun fibers can be modeled simply as classic circumferential buckling of elastic cylindrical shells containing an elastic core under external pressure [32]. The critical buckling pressure p_c can be expressed as [33]

$$p_c = \eta\left[\frac{n^2-1}{3} + \frac{4(1-\upsilon_f^2)(E_s/E_f)(a/t)^3}{(1+\upsilon_s)[2n(1-\upsilon_s)-(1-2\upsilon_s)]}\right]p_0. \tag{1}$$

In equation (1), $\eta = 1 + (1-\upsilon_f^2)/[(1+\upsilon_s)(1-2\upsilon_s)](E_s/E_f)(a/t)$, $p_0 = E_f/[4(1-\upsilon_f^2)](t/a)^3$, n is the wave number of the circumferential surface wrinkles, E_f and E_s are respectively the moduli of the surface layer (film) and core (substrate), ν_f and ν_s are respectively the Poisson's ratios of the film and substrate, t is the film thickness, and a is the radius of the substrate. With the assumption of incompressibility (i.e., $\nu_f = \nu_s = 0.5$), Wang *et al* [32] derived an expression of the critical wave number n_{crit} in minimizing the critical buckling pressure p_c in equation (1) as

$$n_{crit} = (a/t)(3\overline{E}_f/\overline{E}_s)^{1/3}, \tag{2}$$

where $\overline{E}_f = E_f/(1-\upsilon_f^2)$ and $\overline{E}_f = E_f/(1-\upsilon_f^2)$. In addition, Wang *et al* [32] conducted the nonlinear finite element analysis (FEA) to extract the surface wrinkle mode chart in term of the surface morphology (i.e., the wave number n) against the stiffness (E_f/E_s) and aspect ratios (a/t) of the electrospun fibers. Yet, the corresponding critical mismatch strain was not predicted explicitly in their study. Further justification is still needed on how to apply these theoretical predictions for design and optimization of the surface wrinkle modes of electrospun fibers for various practical applications.

As a viable experimental approach, this paper proposes to incorporate hard cores [e.g., carbon nanotubes (CNTs), silica particles, etc] into polymer nanofibers via coaxial electrospinning, i.e., coelectrospinning, to rationally alter the surface wrinkle modes of the resulting core–shell nanofibers. A continuum mechanics model is formulated to explore the dependencies of surface wrinkle modes of the core–shell polymer fibers upon the thickness and stiffness of the glassy shell and inner soft sol-gel layers. Detailed discussions on the wrinkling mechanisms are made and conclusions of the present study are drawn in consequence.

2. Problem statement and solution

Beyond control of the solvent evaporation in electrospinning, herein we formulate a continuum mechanics model to explore the potential of actively altering the surface wrinkle modes of electrospun fibers via introducing a second phase of an artificial hard core. This approach can be realized by means of coelectrospinning, in which hard micro/nanoparticles (e.g., CNTs, silica micro/nanoparticles, etc) can be conveniently enwrapped into the electrospun fibers as the hard core via feeding these hard particles into the inner jet in the coelectrospinning process. Therefore, in the jet whipping stage, the fast drying-induced glassy shell, the inner sol-gel layer and the hard core of enwrapped hard particles can be modeled as a tri-layered cylinder, as illustrated in figure 2, to study the surface wrinkling initiation and regulation. The fast drying (solvent evaporation) of the surface skin (shell) and solvent diffusion in the jet results in the radial solvent-concentration gradient across the jet, leading to the

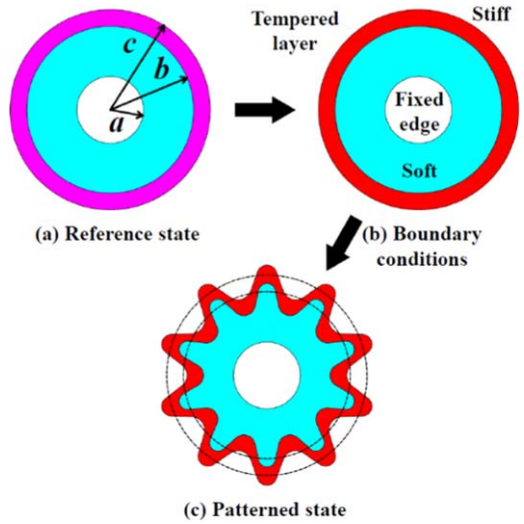

Figure 2. Schematic cross-section of a tri-layered electrospun fiber and surface wrinkling. (*a*) Initial reference state to illustrate the uneven drying, (*b*) boundary conditions, and (*c*) surface wrinkling due to circumferential strain mismatch.

excessive circumferential compressive strain in the initially dried shell and finally triggering surface wrinkling when the critical buckling conditions are reached.

To explore the dependencies of the circumferential wrinkle modes upon the geometries and stiffness of the glassy shell and inner soft sol-gel layer on a hard core in coelectrospinning, nonlinear FEA is utilized for the wrinkling analysis of the present study. During the computational process, the glassy shell and inner soft sol-gel layer of the fiber are modeled as two incompressible hyperelastic neo-Hookean materials with the different shear modulus μ. The strain energy density W of a hyperelastic neo-Hookean material is given as

$$W = \mu/2(\lambda_1^2 + \lambda_2^2 + \lambda_3^2 - 3), \tag{3}$$

where $\mu = \mu_f$ for the glassy shell (film), $\mu = \mu_s$ for the inner sol-gel layer (substrate), and λ_1, λ_2 and λ_3 are the three principal stretches of the fiber along the radial r, circumferential θ, and axial z directions, respectively [34, 35]. Without loss of generality, it is assumed that the fiber is in plane-strain state as any existing axial strain along the fiber axis (z-axis) can be converted into the strains in the fiber cross-section according to material incompressibility of the neo-Hookean solids, which implies $\lambda_1 = 1/\lambda$, $\lambda_2 = \lambda$, and $\lambda_3 = 1$ with λ as a function with respect to r and θ. In reality of electrospinning, axial strain always exists and varies with jet elongation while surface wrinkling happens at the late whipping stage as the shell starts to solidify. By comparison with drying-induced circumferential strain mismatch, the axial strain does not dominate the surface wrinkling process in electrospun fibers. Hereafer, the computational nonlinear buckling (wrinkling) analysis is implemented by using a commercial FEA software package (ANSYS®) as follows. For a typical simulation, given the fiber aspect ratios a/c and t_f/t_s ($t_f = c\text{-}b$ and $t_s = b\text{-}a$), as shown in figure 2(a), and the stiffness ratio μ_f/μ_s of the glassy shell to the inner soft layer, the hard core of radius a is modeled as a rigid body in FEA via applying fixed displacement boundary conditions at the core surface; the initial 'seeded' compressive strains in the glassy shell is made through applying an artificial thermal volumetric strain in the shell. Varying aspect ratios a/c and t_f/t_s as well as stiffness ratio μ_f/μ_s are employed in the compuational simulations to examine the effects of the hard core of varying radius and the polymer-solvent system of varying solvent fraction and evaporation rate in coelectrospinning. Numerical results gained from the computational simulation include the minimum critical compressive strain (ε_c) in the glassy shell and the corresponding wave number n of the surface wrinkle modes. In a realistic coelectrospinning process, the aspect ratios a/c and t_f/t_s and stiffness ratio μ_f/μ_s are governed by the process parameters, polymer-solvent system, and the jet drying rate, which further determine the residual compressive strain ε_r (i.e., the circumferential strain mismatch) in the glassy shell. Once ε_r in the shell is equal or larger than the critical wrinkling strain ε_c to evoke circumferential surface wrinkling, the predicted wrinkle mode with the wave number n is expected observable in electrospinning, as illustrated in figure 2(c).

During the computational simulation, a variety of combinations of the aspect ratios (a/c and t_f/t_s), as shown in figure 3, and stiffness ratio (μ_f/μ_s) are employed to examine the parameter effects of varying drying rates and polymer-solvent systems in the sense of physics. Two values of a/c (i.e., 0.25 and 0.75) are considered to represent two types of hard core, i.e., small- and large-sized hard cores; for each a/c, four values of t_f/t_s (i.e., 0.1, 0.25, 0.5, and 1.0) are utilized to stand for four different types of polymer-solvent systems (with varying drying rates). Furthermore, for each combination of a/c and t_f/t_s, three values of μ_f/μ_s (i.e., 10, 100, and 1,000) are employed in the computational simulations. As aforementioned, the values of t_f/t_s and μ_f/μ_s are employed to

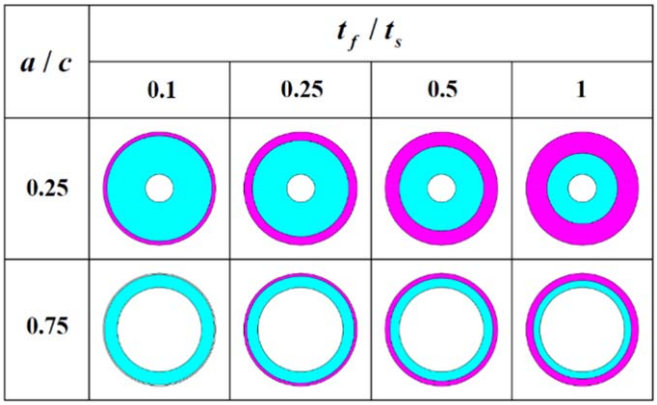

Figure 3. Schematic cross-section geometries of electrospun core–shell fibers of varying aspect ratios a/c and t_f/t_s used in computational wrinkling analysis.

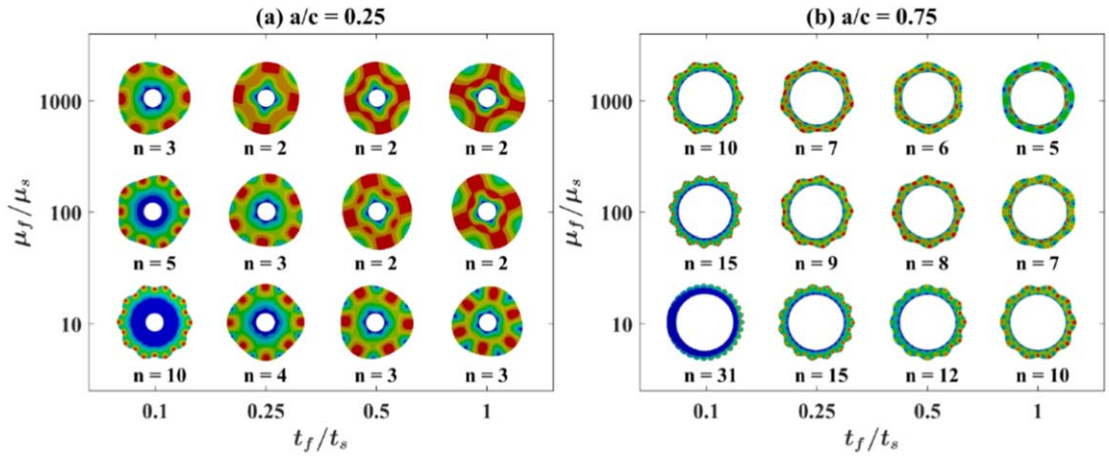

Figure 4. Critical surface wrinkle mode charts in term of the wave number n and surface topology against the aspect ratio t_f/t_s and stiffness ratio μ_f/μ_s. (*a*) a/c = 0.25 and (*b*) a/c = 0.75.

phenomenologically represent the relevant geometrical and elastic properties of the polymer-solvent system in coelectrospinning as the exact dependency is not available yet from the literature. Figure 4 shows the critical surface wrinkle mode charts in term of the wave number n (the lowest) and surface topology against the aspect ratio t_f/t_s and stiffness ratio μ_f/μ_s for $a/c = 0.25$ and 0.75, respectively, in which the color contours of wrinkled fiber cross-sections represent the in-plane characteristic deformations in the fiber cross-section after wrinkling (i.e., eigen-deformation). It can be observed from figure 4 that given the size of a hard core (a/c), the wave number n (i.e., the number of surface wrinkles) decreases from $n = 10$ to 3 with increasing either stiffness ratio μ_f/μ_s from 10 to 1,000 or fiber aspect ratio t_f/t_s from 0.1 to 1. This observation has a clear physical picture in coelectrospinning as a high stiffness ratio μ_f/μ_s and/or a high fiber aspect ratio t_f/t_s are directly correlated to a high gradient of solvent concentration across the fiber, i.e., a fast solvent evaporation (drying), which generally leads to a shaped electrospun fiber with fewer surface wrinkles (i.e., a lower value of the wave number n) as evidenced in electrospinning experiments [21, 22, 32]. In addition, within the framework of continuum mechanics [32, 33], it has been showed that once buckled, a stiffer and thicker surface layer attached onto a compliant substrate under in-layer compression generally generates surface wrinkles with a smaller wave number n, *i.e.,* a large wavelength. As a conclusion, reduction of the solvent evaporation rate (drying rate) in electrospinning or more even drying across the jet (i.e., the lower μ_f/μ_s and t_f/t_s ratios) generally produces micro/nanofibers with more wrinkled surfaces (i.e., a higher wave number n).

Furthermore, comparison between figures 4(a) and (b) shows that adoption of a hard core in coelectrospinning can significantly alter the surface wrinkling of electrospun fibers. At fixed t_f/t_s and μ_f/μ_s, i.e., the similar process parameters and polymer-solvent systems used in coelectrospinning, a large-sized hard core can trigger a larger wave number n, and the n-a/c correlation is roughly linear. This observation can be understood such that more surface wrinkles (with larger bending curvature and flexural energy) are needed to

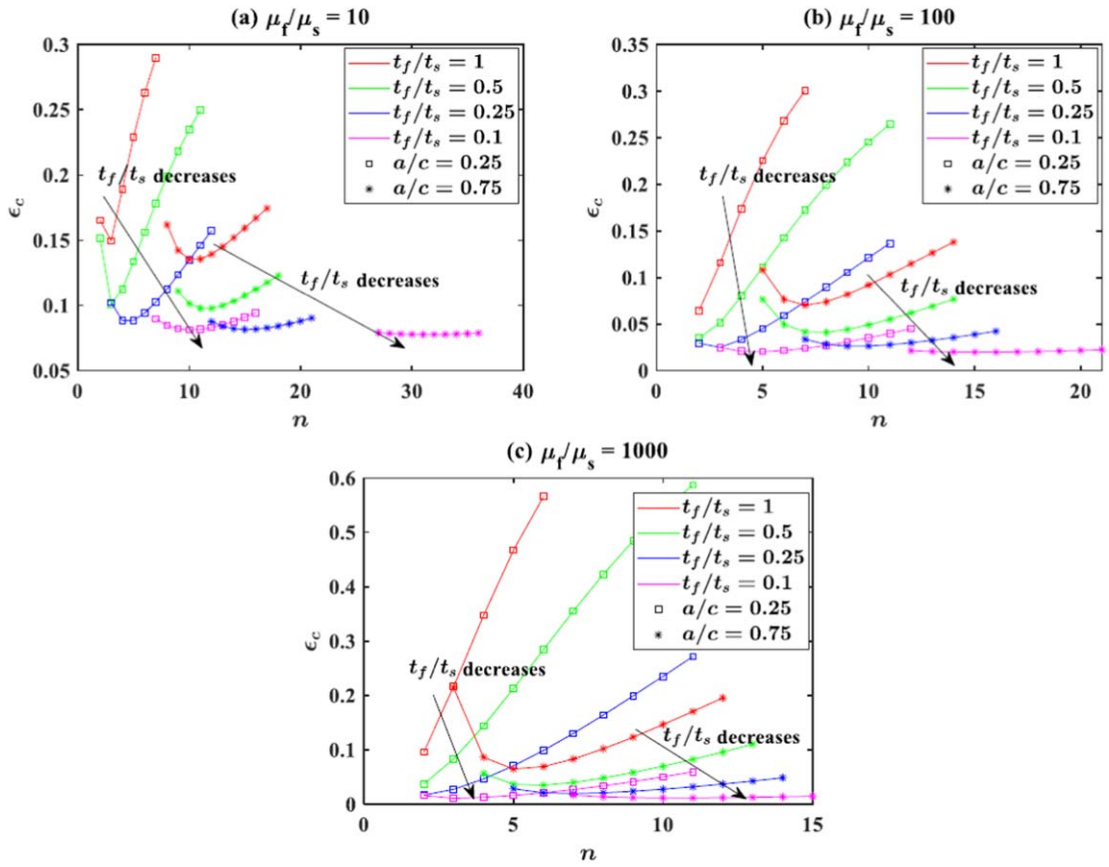

Figure 5. Variation of the critical wrinkling strain ε_c with respect to the wave number n of the surface wrinkle modes at varying aspect ratios t_f/t_s and a/c. (*a*) $\mu_f/\mu_s = 10$, (*b*) $\mu_f/\mu_s = 100$, and (*c*) $\mu_f/\mu_s = 1{,}000$.

store the strain energy released from the compressed glassy shell upon surface wrinkling in the electrospun fibers with a large-sized hard core (i.e., with relatively thinner polymer layers). Thus, the surface wrinkle modes of electrospun fibers can be actively tuned via adjusting the size of the hard core in coelectrospinning.

Figure 5 further shows the variation of the critical wrinkling compressive strain ε_c in the glassy shell with respect to the wave number n, i.e., the characteristic wrinkling ε_c-n diagram, at varying aspect ratios $t_f t_s$ and a/c and stiffness ratio μ_f/μ_s of electrospun fibers with hard cores as shown in figure 3. Figure 5 is extracted from the computational simulations for the surface wrinkle mode charts as shown in figure 4. At fixed values of a/c (i.e., fixed size of the hard core) and μ_f/μ_s, figure 5 indicates that ε_c in the glassy shell decrease rapidly with deceasing t_f/t_s, i.e., the thinner the glassy shell is (fast drying), the easier the surface wrinkling happens, which is correlated to the experimental observations [21, 22, 32]. In principle, the wrinkling of a thin elastic layer on a compliant substrate depends upon the flexural stiffness of the layer in term of $\sim \mu t_f^{\,3}$; this cubic relation with respect to the layer thickness is roughly followed in figure 5. In addition, for relatively thick glassy shells (e.g., $t_f/t_s = 0.25, 0.5,$ and 1.0) of the electrospun fibers with a small-sized hard core ($a/c = 0.25$), ε_c increases nearly linearly with increasing wave number n; however, ε_c becomes insensitive to n for $t_f/t_s = 0.1$. In the case of the electrospun fibers with a large-sized core ($a/c = 0.75$), except for the case of $t_f/t_s = 1.0$, ε_c becomes insensitive to n for $t_f/t_s = 0.1, 0.25$ and 0.5. These observations show that fast drying (i.e., the thinner glassy shell or lower t_f/t_s) and large-sized hard core (i.e., larger a/c) typically result in a smaller ε_c, which is also insensitive to n, i.e., surface wrinkles corresponding to multiple values of n can coexist similar to multiple standing surface waves of varying wave length/number. In addition, in the case of the electrospun fibers with large-sized hard cores (i.e., large values of a/c), the characteristic wrinkling ε_c-n diagram behaves concave, implying that in the solvent evaporation process, the wave number n has the behavior of bifurcation with respect to ε_c. This bifurcation behavior can be understood such that with fast solvent evaporation from the jet, the compressive residual strain ε_r in the glassy shell grows and then exceeds the minimum ε_c, which may potentially trigger the surface wrinkling of two types of wrinkle mode. In addition, ε_c of electrospun fibers with small-sized hard cores (i.e., small values of a/c) behaves more sensitive to μ_f/μ_s than that of electrospun fibers with large-sized hard cores. As a conclusion, the ε_c-n diagrams of electrospun fibers at varying a/c, t_f/t_s and μ_f/μ_s provide a complete scenario of the dependencies of surface wrinkle modes upon the process and material parameters adopted in

coelectrospinning, which can be considered as the guidelines for surface wrinkling control and optimization. Furthermore, in the present computational study, the actual inhomogeneous fiber cross-section is modeled as two-layered coaxial structure with varying thickness ratio and stiffness ratio to approach the stiffness gradient in the realistic fiber cross-section. In such a simplification scheme, the stiffness of two-layered coaxial structure of the fiber is understood as a rational phenomenological approach of the effective stiffness of the inhomogeneous portion of the fiber section, which would not result in noticeable errors in the modeling.

Consequently, it needs to be mentioned that the typical diameters of electrospun fibers are in the range of a few nanometers to micrometers. Within such small scales, surface tension/energy of compliant electrospun fibers may influence their mechanical behavior [25, 26, 36–40] and related critical wrinkling strain ε_c and surface wrinkle modes (the wave number n). As surface effects (e.g., surface tension/energy, etc) are excluded in the present study, the present computational scaling analysis indicates that the wrinkled surface topologies (i.e., the wave number n) only depends upon the aspect ratio (a/c and t_f/t_s) and stiffness ratio (μ_f/μ_s) while explicitly independent of the fiber radius c, i.e., the surface wrinkling phenomenon within the present continuum mechanics framework is size-independent. Therefore, all the numerical results gained above and conclusions drawn from this study are applicable to surface wrinkling analysis of all types of compliant fibers and cylinders with hard cores.

3. Concluding remarks

Wrinkle modes of ultrathin polymer fibers produced in electrospinning process can be conveniently regulated via incorporating hard cores into the fibers. The dependencies of surface wrinkle modes of these core–shell polymer fibers enwrapped with hard cores upon the thickness and stiffness ratios of the glassy shell and inner soft sol-gel layer have been obtained via detailed nonlinear computational buckling analysis, which provide a rational basis of producing ultrathin polymer micro/nanofibers with controlled surface morphologies. Such electrospun nanofibers carry greatly enhanced specific surface areas suitable for various advanced applications including oil-water separation, high-graded gas and liquid filtration, drug delivery, catalyst carriers, tissue scaffolding, etc.

Acknowledgments

Partial support of the research by the National Science Foundation (Award No.: CMMI-1234297), NDSU Development Foundation (FAR0021589), DOE and Department of Mechanical Engineering at North Dakota State University is gratefully acknowledged. The electrospun PS fibers shown in figure 1 were prepared by former graduate student Z Zhou in the group.

ORCID iDs

Mojtaba Ahmadi https://orcid.org/0000-0002-6735-970X
Xiang-Fa Wu https://orcid.org/0000-0003-2008-7564

References

[1] Reneker D H and Chun I 1996 *Nanotechnology* **7** 216
[2] Reneker D H, Yarin A L, Zussman E and Xu H 2007 *Adv. Appl. Mech.* **41** 43
[3] Reneker D H and Yarin A L 2008 *Polymer* **49** 2387
[4] Dzenis Y 2004 *Science* **304** 1917
[5] Li D and Xia Y N 2004 *Adv. Mater.* **16** 1151
[6] Kim J S and Reneker D H 1999 *Polym. Compos.* **20** 124
[7] Gibson P, Schreuder-Gibson H and Rivin D 2001 *Colloids Surf.* A **187** 469
[8] Huang Z M, Zhang Y Z, Kotaki M and Ramakrishna S 2003 *Compos. Sci. Technol.* **63** 2223
[9] Lai C, Guo Q H, Wu X F, Reneker D H and Hou H 2008 *Nanotechnology* **19** 195303
[10] Schulz D L *et al* 2010 *Electrochem. Solid State Lett.* **13** A143
[11] Sinha-Ray S, Pelot D D, Zhou Z P, Rahman A, Wu X F and Yarin A L 2012 *J. Mater. Chem.* **22** 9138
[12] Wu X F, Rahman A, Zhou Z, Pelot D D, Sinha-Ray S, Chen B, Payne S and Yarin A L 2013 *J. Appl. Polym. Sci.* **129** 1283
[13] Wu X F and Yarin A L 2013 *J. Appl. Polym. Sci.* **130** 2225
[14] Mohammadzadehmoghadam S, Dong Y and Davies I J 2015 *J. Polym. Sci. B: Polym. Phys.* **53** 1171
[15] Reneker D H, Yarin A L, Fong H and Koombhongse S 2000 *J. Appl. Phys.* **87** 4531
[16] Yarin A L, Koombhongse S and Reneker D H 2001 *J. Appl. Phys.* **89** 3018
[17] Shin Y M, Hohman M M, Brenner M P and Rutledge G C 2001 *Appl. Phys. Lett.* **78** 1149
[18] Hohman M M, Shin M, Rutledge G and Brenner M P 2001 *Phys. Fluids* **13** 2221
[19] Bognitzki M, Czado W, Frese T, Schaper A, Hellwig M, Steinhart M, Greiner A and Wendorff J H 2001 *Adv. Mater.* **12** 70

[20] Dayal P, Liu J, Kumar S and Kyu T 2007 *Macromolecules* **40** 7689
[21] Koombhongse S, Liu W and Reneker D H 2001 *J. Polym. Sci. Part B: Polym. Phys.* **39** 2598
[22] Pain C L, Boyce M C and Rutledge G C 2009 *Macromolecules* **42** 2102
[23] Naraghi M, Chasiotis I, Kahn H, Wen Y K and Dzenis Y 2007 *Appl. Phys. Lett.* **91** 151901
[24] Naraghi M, Chasiotis I, Kahn H, Wen Y and Dzenis Y 2007 *Rev. Sci. Instrum.* **78** 085108
[25] Wu X F, Kostogorova-Beller Y Y, Goponenko A V, Hou H W and Dzenis Y A 2008 *Phys. Rev.* E **78** 061804
[26] Wu X F 2010 *J. Appl. Phys.* **107** 013509
[27] Tang S, Li Y, Liu W K, Hu N, Peng X H and Guo Z 2015 *J. Appl. Mech. -Trans. ASME* **82** 121002
[28] Wu X F, Salkovskiy Y and Dzenis Y A 2011 *Appl. Phys. Lett.* **98** 223108
[29] Yu M 2012 *Experimental and Computational Studies of Immiscible Droplets Wetting on Micro and Nanofibrous Materials and Their Applications in Oil-water Separation (Thesis)* (North Dakota, USA: North Dakota State University)
[30] Zhou Z and Wu X F 2015 *Mater. Lett.* **160** 423
[31] Zhou Z, Lin W and Wu X F 2016 *Colloids Surfaces A: Physicochem. Eng. Asp.* **494** 21
[32] Wang L, Pai C L, Boyce M C and Rutledge G C 2009 *Appl. Phys. Lett.* **95** 15191
[33] Herrmann G and Forrestal M J 1965 *AIAA J.* **3** 1710
[34] Zhao R and Zhao X 2017 *J. Appl. Mech.* **84** 081001
[35] Cowin S C and Doty S 2007 *Tissue Mechanics* (New York: Springer)
[36] Wu X F and Dzenis Y A 2006 *J. Appl. Phys.* **100** 124318
[37] Wu X F and Dzenis Y A 2007 *J. Appl. Phys.* **102** 044306
[38] Wu X F and Dzenis Y A 2007 *Nanotechnology* **18** 285702
[39] Wu X F and Dzenis Y A 2007 *J. Phys. D: Appl. Phys.* **40** 4296
[40] Wu X F, Bedarker A and Akhatov I S 2010 *J. Appl. Phys.* **108** 083518